nature physics

LETTERS

https://doi.org/10.1038/s41567-021-01335-8

Check for updates

The cusp of an apple

Aditi Chakrabarti[1,5], Thomas C. T. Michaels[1,2,5], Sifan Yin[1,3], Eric Sun[1] and L. Mahadevan[1,4]✉

Singularities are common in diverse physical systems[1] and lead to universal structures[2,3]. This universality suggests that they should also naturally arise in biological systems, where active growth, autonomous motion, kinesis and taxis focus deformations in spacetime, as exemplified in the morphogenetic processes determining biological size and shape[4]. A familiar example of a morphogenetic singularity is seen in the humble apple, which forms in the neighbourhood of the stalk as the apple grows. Here we study the geometry and morphogenesis of the cusp of an apple by combining observations of fruit growth with a simple theory, finite element simulations and controlled swelling experiments using a physical gel simulacrum. Our observations show that the axisymmetric cusp develops into a self-similar form, which can be understood in terms of a mechanical theory for the inhomogeneous growth of a soft sphere. Physical experiments using local inhibition in swelling gels corroborate our theoretical predictions. These experiments further show that axisymmetric cusps can lose stability and become lobed. We use simulations to show that the number of cuspidal lobes depends on the ratio of the size of the stalk to the size of the sphere, as well as the amplitude and periodicity of perturbations that mimic the role of fruit anatomy, consistent with observations of multi-cusped fruits.

A longitudinal cross-section of a mature apple reveals its anatomy (Fig. 1a): the innermost seed cavity forms a stiff core encapsulated by a fleshy cortex that is surrounded by a thin epidermal layer, that is, the skin. The fruit is suspended from a branch via a stalk, which also serves as a transport channel from the tree during its growth. A network of vascular bundles[5] in the cortex further distributes the nutrients and water received from the stalk to the tissues during fruit growth. Following pollination and fertilization of the ovules at the base of the flower[6,7], the petals fall off, while the ovary and fleshy cortex expand going through several rounds of cell division during the first month after anthesis[8]. During this stage, there is no visible cusp around the stalk. This first stage is followed by a prolonged phase over several weeks, where the fruit increases in size mainly due to cell expansion and addition of starch and sugar metabolites. Quantitative measurements indicate that the cells and intercellular spaces in the cortex expand much more than the outer epidermis and inner core[7,9–12] (Supplementary Fig. 3). While the cortex grows at a much faster rate than the core, the latter shows some growth during the later stages of apple development[7]. It is during this cortical expansion phase that the cusp at the stalk begins forming and achieves its final shape (see Fig. 1 in ref. [8] for the developmental timeline of a fruit). All together, these observations of apple growth suggest that its cusp arises due to differential expansion between the cortex that grows in volume fivefold than the core[13], with hindered growth at the stalk. Furthermore, the density of vascular channels is much higher in the cortex than in the core or epidermal regions[5], directly showing that water and nutrients are preferentially added to the cortex.

To experimentally follow the formation of the cusp, we directly estimated the growth profile of apples picked at various growth stages in the orchard of Peterhouse, University of Cambridge, UK, during June 2018. The profile of the cusp was determined by longitudinally cutting the apples at the stalk. Therefore, instead of watching a single apple grow as a function of time, we imaged the longitudinal cross-section of the apples at various stages. This procedure resulted in a pseudo-ontogenetic time course of growth of an apple cusp, as shown in Fig. 1b (Extended Data Fig. 1a). In the experiments, we observed that apples smaller than about 1.5 cm in diameter did not exhibit a detectable cusp. In contrast, larger apples (diameter, >3 cm) exhibited a cusp with shape profile $y(x)$ measured relative from the distance to the stalk, x. This is consistent with previous observations of commercial apple varieties, showing that the cusp becomes apparent about 30 days after full bloom when the diameter is about 2 cm (refs. [8,13]).

To understand the evolution of the shape of the apple in the neighbourhood of the cusp, we turn to singularity theory[1,2]. Defining the profile of the apple as a one-dimensional curve represented parametrically using arc length s as $\mathbf{x}(s) = (x(s), y(s))$, where $x(s)$ is the horizontal distance from the stalk and $y(s)$ is the height (that can be used to generate a solid of revolution around the stalk) (Fig. 1a), we expand these functions in a Taylor series in s (the distance from the stalk). Noting that the fruit profile has mirror symmetry about the stalk, that is, $x(-s)=-x(s)$ and $y(-s)=y(s)$, implies that $x(s)=x_1 s+x_3 s^3+\ldots$ and $y(s)=y_2 s^2+\ldots$. When $x_1=0$, this yields $y(s)\simeq y_2 s^2$ and $x(s)\simeq x_3 s^3$—corresponding to an ideal cusp $y\propto x^{2/3}$ (Supplementary Fig. 1c). For $x_1>0$, the fruit profile is cusp-like from afar (that is, when $s\gg(x_1/x_3)^{1/2}$), but it is regularized to be parabolic when viewed closely (that is, when $s\ll(x_1/x_3)^{1/2}$) (Supplementary Fig. 1b); indeed, when $x_3=0$, the fruit profile is parabolic, that is, $y\propto x^2$. We see that simple symmetry considerations lead to the surface being spherical on large scales, a self-similar cusp on intermediate scales and a regularized parabola on very small scales, as seen in similar interfacial structures in simple fluids and solids[1,14]. Indeed, using $s=\sqrt{y/y_2}$, we obtain $x=x_1\sqrt{y/y_2}+x_3\sqrt{(y/y_2)^3}$; close to the stalk, we can, therefore, write the fruit profile in a self-similar form as

$$ay(x) = H(bx), \quad a = x_3/(y_2 x_1), \quad b = \sqrt{x_3/x_1^3}, \tag{1}$$

where the self-similar function $H(\xi)$ is defined as

$$\sqrt{H}(1+H) = \xi. \tag{2}$$

Thus, by appropriate rescaling of the x and y axes to $y^*=ay$ and $x^*=bx$, fruit profiles near the cusp (Fig. 1c) are expected to collapse

[1]Harvard John A. Paulson School of Engineering and Applied Sciences, Harvard University, Cambridge, MA, USA. [2]Department of Physics and Astronomy, Institute for the Physics of Living Systems, University College London, London, UK. [3]Institute of Biomechanics and Medical Engineering, Department of Engineering Mechanics, Tsinghua University, Beijing, People's Republic of China. [4]Department of Physics, Department of Organismic and Evolutionary Biology, Harvard University, Cambridge, MA, USA. [5]These authors contributed equally: Aditi Chakrabarti, Thomas C. T. Michaels. ✉e-mail: lmahadev@g.harvard.edu

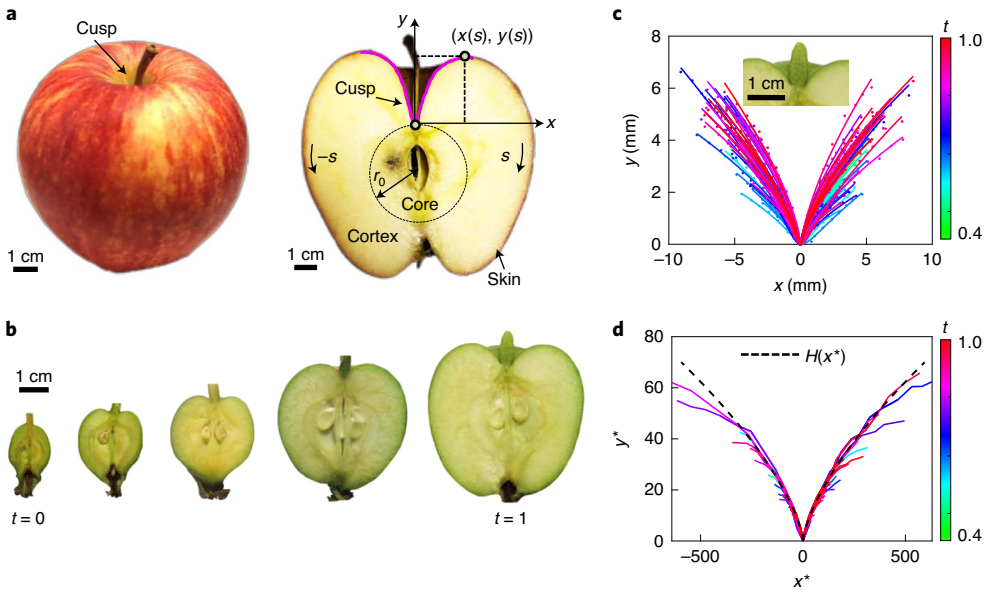

Fig. 1 | Experimental observations of the growth and form of the cusp of an apple. a, A Gala apple with a cusp where the fruit meets the stalk. Its longitudinal mid-plane cross-section shows the curve $\mathbf{x}(s) = (x(s), y(s))$ depicting the shape near the stalk, where s is the arc length and $x(s)$ and $y(s)$ are the coordinates of the apple cusp profile relative to the origin set at the end of the stalk, respectively. The initial core size is r_0. **b**, Experimental measurements of apple cross-sections at different stages of growth, where t depicts the effective time course—a proxy for the different stages of apple growth. **c**, Apple growth profile $\mathbf{x} = (x, y)$ near the stalk, measured for each apple at time t. The inset shows an enlarged version of the cusp of a mature apple ($t = 1$). The apple profiles were traced from the images of a total of 100 apples picked at different stages of growth. **d**, Apple growth profiles are rescaled according to $y^* = ay$ and $x^* = bx$, where a and b are defined in equation (1). The rescaled profiles collapse onto a single universal curve $y^* = H(x^*)$ predicted by the singularity theory (dashed line; equation (2)).

onto the universal curve $y^* = H(x^*)$, which is in excellent agreement with the measured apple profiles shown in Fig. 1d.

To complement the geometric picture, we consider a minimal dynamical picture of the growth of the apple as that of a moving interface, with a local velocity that depends only on the local geometry. If there is a spherical front corresponding to the surface of the apple, a cusp will form if there is a source of a chemical that inhibits growth and has an influence that is due to a balance between diffusion and degradation over time, leading to a free boundary problem for the shape of an accreting material in the neighbourhood of a point source of inhibitor. The simplest mathematical description of the above process leads to the eikonal equation[1]. By virtue of the azimuthal symmetry of the problem, we can confine ourselves to a two-dimensional surface parameterized in polar coordinates as $\mathbf{x} = (x, y) = (r\cos\varphi, r\sin\varphi - r_0)$, where $r(\varphi,t)$ describes the growing front, where φ is the angular coordinate, r_0 is the initial radius, and the eikonal equation becomes $\frac{\partial r}{\partial t} = c\sqrt{1 + \frac{1}{r^2}\left(\frac{\partial r}{\partial \varphi}\right)^2}$. If the prescribed normal velocity c is constant, an initially spherical profile will continue to maintain its spherical shape with time. Instead, if growth is restricted at the stalk and tends to a constant value away from the stalk (over a characteristic length scale controlled by the diffusion of a growth inhibitor and growth speed), a self-similar cusp develops from the eikonal equation only after a finite time and critical size (Supplementary Section 1 and Supplementary Fig. 2), just as observed in apples (Fig. 1c,d).

The geometric and dynamical theory presented above are generic—they do not depend on any molecular, cellular or physical details of the growth process. However, observations[7] (Supplementary Fig. 3) of differential growth between the cortex and core coupled with the fact that the apple grows everywhere except near the stalk region and inner core suggest a mechanical basis for cusp formation in the apple. To quantify this, we model the apple as a growing neo-Hookean material with a volumetric strain energy density $W_A = \frac{\mu}{2}\left[J_A^{-\frac{2}{3}}\mathrm{Tr}(\mathbf{A}\cdot\mathbf{A}^T) - 3\right] + \frac{K}{2}(J_A - 1)^2$, where $\mathbf{A}$ is the elastic deformation gradient, $J_A = \det\mathbf{A}$, μ is the shear modulus and K is the bulk modulus, assumed to be $O(10^3\mu)$, that is, the tissue is almost incompressible. The deformation gradient is multiplicatively decomposed into an elastic part and a growth part $\mathbf{F} = \mathbf{AG}$. To model isotropic inhomogeneous growth, we use the following profile: $\mathbf{G} = g(x,y,t)\mathbf{I}$, $\mathbf{I}$ being the identity matrix and the growth rate is given by $g(x,y,t) = 1 + f(R)h(d)t$, with $f(R) = \{1 + \exp[-k_R(R - R_{cr})/R_0]\}^{-1}$ and $h(d) = \{1 + \exp[-k_d(d - d_{cr})/d_0]\}^{-1}$, where R_0 is the initial radius of the apple, R_{cr} is the radius of the non-growing core and d_{cr} is the radius of the stalk. Here $R = \sqrt{x^2 + (R_0 + y)^2}$, $d = \sqrt{x^2/d_a^2 + y^2/d_b^2}$ and $d_0 = R_0\sqrt{1/d_a^2 + 1/d_b^2}$. This growth profile allows g to vary smoothly from $g = 1$ in the core and the neighbourhood of the stalk to $g > 1$ in the outermost cortex, similar to the the growth profiles that drive the form of cortical convolutions in the human brain[15]. Both axisymmetric and three-dimensional simulations are performed using the commercial finite element program Abaqus/Standard v. 6.14 (ref. [16]), minimizing the elastic energy. In Fig. 2a,b, we see that our computations capture the formation of an axisymmetric cusp with the self-similar form expected from the singularity theory, while providing a simple mechanical basis for its origin (Extended Data Figs. 1b and 2). The universal self-similar scaling holds for both cases of a cortical growth front moving inwards and a cortical growth front moving outwards from the core–cortex interface (Supplementary Fig. 4), suggesting that non-polar differential growth between the cortex and pith suffices to create a cusp.

With our understanding of the cusp using field experiments in apples, theory and computation, a natural question is that of lab

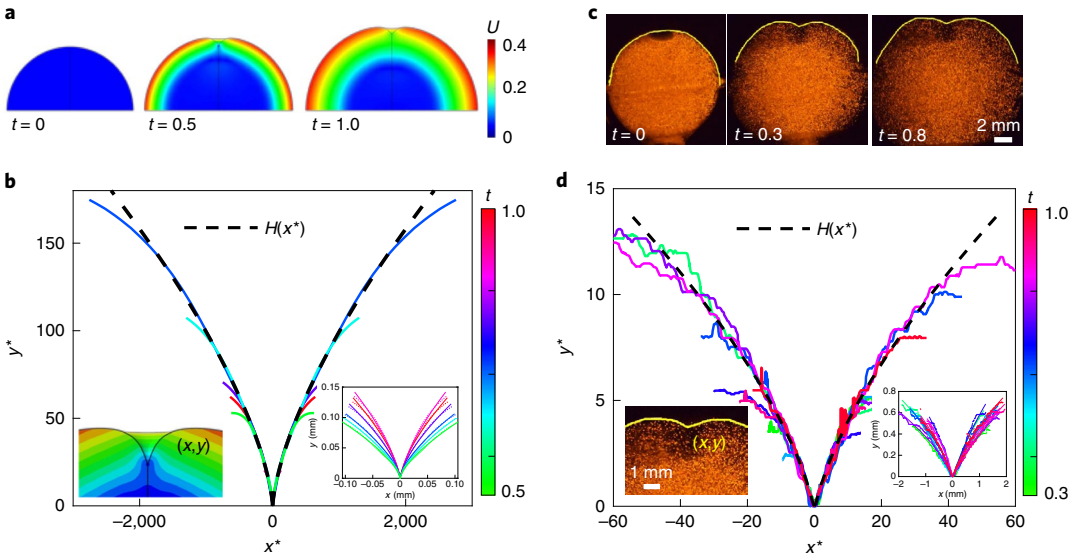

Fig. 2 | Numerical simulations of a growing solid and physical experiments with swelling gels recapitulate axisymmetric cusp formation. a, Finite element simulations of a growing hyperelastic sphere with a small zone of inhibited growth near the pole, showing cusp formation. The colour bar represents the displacement magnitude (U), and t represents the normalized time relative to the final time at which the cusp is fully developed. **b**, Universal self-similarity of the rescaled profiles of cusps from the finite element simulations $y^* = ay$ and $x^* = bx$, which are superimposed with the curve $y^* = H(x^*)$ (dashed line) (equations (1) and (2)). The left inset shows a magnified version of the cusp at $t = 0.5$. The right inset shows the cusp profiles (x,y) obtained from the finite element simulations measured relative to the origin set at the upper central part of the model, that is, the 'stalk'. **c**, Laser sheet imaging of the swelling of a spherical gel of PDMS with a non-swelling 'stalk' made with co-curing a drop of a fluoroelastomer (1:1) at the north pole of the gel model. The PDMS gel was embedded with polyethylene fluorescent spheres (0.3 w/w%; diameter, ~35–40 μm) to visualize the central cross-section of the model during its growth when submerged in a jar of hexane. This enabled the imaging of the cusp profile during the time course of growth due to swelling and visualizing the evolution of the cusp, where t represents the normalized time relative to the final time at which the cusp is fully developed. **d**, Universal self-similarity of the rescaled profiles of the gel cusps are plotted using rescaled axes $y^* = ay$ and $x^* = bx$ in the same way as in **b** (see equations (1) and (2)). The left inset shows a magnified version of the gel cusp at $t = 0.8$. The right inset shows the cusp profiles (x,y) measured at the stalk for these gel models as they grow as a function of time.

experiments to mimic the process of cusp formation. To do so, we fabricated gel spheres made of a polymer (polydimethylsiloxane (PDMS), 40:1) swellable in hexane, with a 'stalk' on its pole made of a different polymer that does not swell in hexane (fluoroelastomer SIFEL8070, 1:1; further details in Methods). If the ratio of the initial stalk diameter (D_{stalk}) to the initial sphere diameter (D_{sphere}) was small enough, that is, $D_{stalk}/D_{sphere} < 0.1$, an axisymmetric singular cusp forms within an hour of swelling in hexane (for an initial $D_{sphere} = 12$ mm chosen to mimic a young apple) (Fig. 2c). On swelling the gel sphere in hexane, the solvent migrates inwards from the boundary of the sphere. Over time, three morphologically distinct zones develop, as revealed by the laser sheet images: an outer zone that is fully swollen, an intermediate zone that is partially swollen and an inner 'unswollen' core, similar to what is seen in an apple[7]. The shape of the cusp $y(x)$ near the stalk is obtained from the profiles of the laser sheet imaging of the embedded fluorescent particles (Extended Data Fig. 1c). On rescaling the coordinates using the form $y^* = ay$ and $x^* = bx$ (as defined earlier), the resulting profiles collapse onto a universal curve $y^* = H(x^*)$ corresponding to a self-similar axisymmetric cusp arising from the singularity theory (Fig. 2d).

Although we have focused on axisymmetric cusps so far, casual observations show that apples can have non-axisymmetric cusps (Fig. 3a). A biologically plausible explanation for this is that the carpel number, which is intrinsic to the fruit anatomy, determines the number of cusps due to hindered growth along the carpel junctions[17]. However, we see the number of cusps ranging from $n = 1$ to $n = 7$ in a range of apple species such as Gala, Honeycrisp and Red Delicious (Fig. 3a), even though all of them have exactly five carpels. This suggests a role for a mechanical basis of number of cusps that operates in parallel with carpel anatomy. To understand the interplay between mechanical instabilities and intrinsic fruit anatomy, we performed numerical simulations of multi-cusp formation with hindered growth at the stalk region by varying the D_{stalk}/D_{sphere} ratios.

We captured the role of carpel anatomy by prescribing an initial perturbation to the shape of the growing spheroid in terms of a vertical displacement of the form $U_y(r,\theta) = Ar\cos(m\theta)$, where θ is the azimuthal angle, m is a prescribed periodicity equal to the carpel number (Fig. 3b) and A is the scaled amplitude of this carpel-induced surface growth (assumed to be the same for all values of m for simplicity). We allowed for the growth of the hyperelastic sphere for different values of the scaled amplitude A, leading to the phase diagram shown in Fig. 3c. For small amplitudes, we consistently observed the formation of a single cusp irrespective of the initial periodicity m. For large amplitudes, the final number of cusps (n) was solely determined by m; we interpret this regime as corresponding to the case under an external perturbation, that is, the carpel number determines the number of cusps. Interestingly, we found an intermediate regime where we observe stable multi-cusped shapes, whose number is independent of m but depends on the D_{stalk}/D_{sphere} ratio.

To corroborate our simulations, we also carried out experiments of swelling gels with different initial D_{stalk}/D_{sphere} ratios in hexane (Fig. 3d) and also observe the formation of multiple cusps (n) for $D_{stalk}/D_{sphere} > 0.1$. A cutting experiment of the swollen gel sphere provides the mechanism for the formation of multiple cusps: as the swelling zone progresses inwards in the neighbourhood of the cusp, the geometry of the spheroid causes an overturning and compression of the outer zone that is already swollen (Extended Data Fig. 3b),

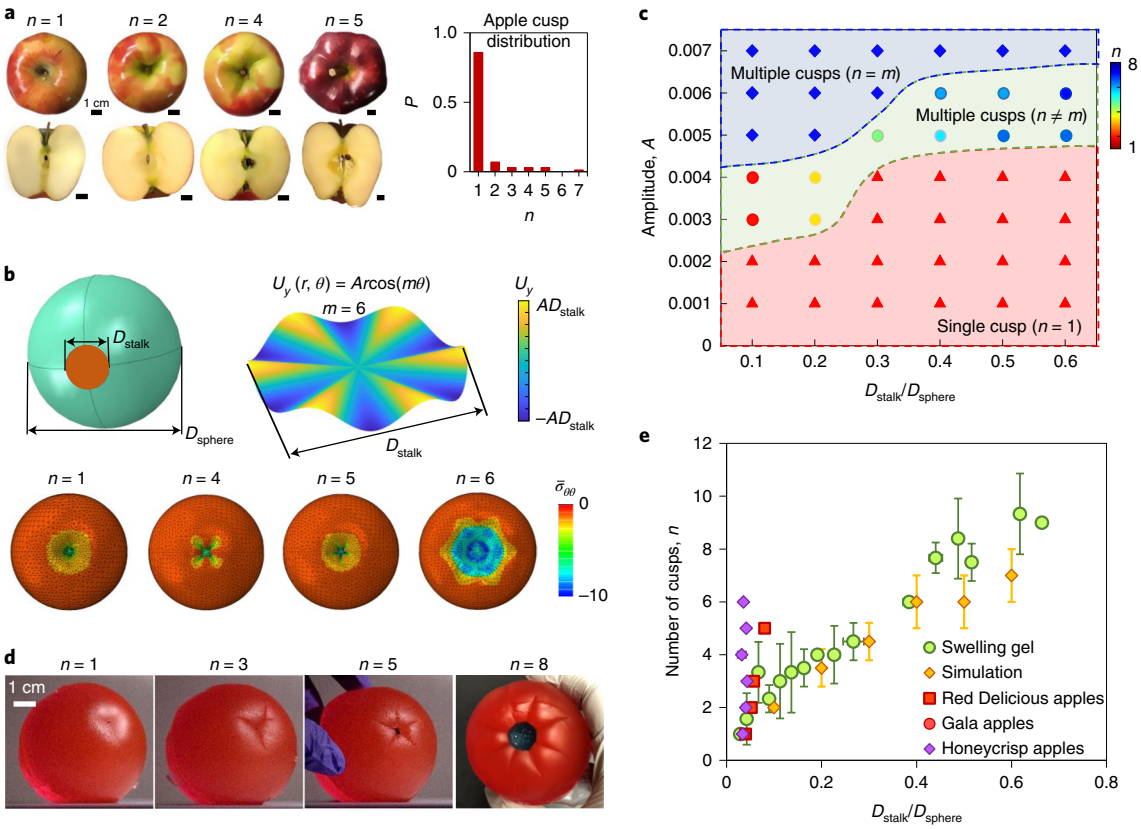

Fig. 3 | Instability of an axisymmetric cusp can lead to multi-cusped forms. a, Plan views and mid-plane cross-sections of apples with multiple cusps: $n=1$ (Gala), $n=2,4$ (Honeycrisp) and $n=5$ (Red Delicious). Right: histogram for ratio (P) of apples with various number of cusps (n) measured for Gala, Honeycrisp and Red Delicious (total, 123 apples). **b**, Schematic of a finite element model setup of a sphere (diameter, D_{sphere}) with growth inhibited in the stalk (diameter, D_{stalk}). Right: an example of a sinusoidal perturbation with amplitude AD_{stalk} and periodicity $m=6$ for initiating multi-cusped forms in simulations. Bottom: simulations showing multi-cusped forms with an increasing number of cusps ($n=1,4,5,6$). The colour bar represents the circumferential stress $\bar{\sigma}_{\theta\theta}$. All the simulations are performed via a four-step growth model (Extended Data Fig. 2d). **c**, Phase space of scaled amplitude (A) versus D_{stalk}/D_{sphere} shows multistability in numerical simulations with different regimes: for low A, we get a single cusp $n=1$; for intermediate A, we get multi-cusped forms with $n\neq m$ (colour bar in the legend corresponds to this intermediate regime); for large A, we get multi-cusped forms where the prescribed periodicity determines the final number of cusps, $n=m$. **d**, A spherical PDMS gel dyed with a red pigment—with an inhibition zone ('stalk') of SIFEL fluoroelastomer dyed with a green pigment—grows due to swelling in hexane. Experiments with varying 'stalk' diameters change the number of cusps ($n=1,3,5,8$) with an increase in stalk size (D_{stalk}). **e**, Number of cusps (n) for apples (Gala, Honeycrisp and Red Delicious), swelling gels and numerical simulations (corresponding to the intermediate regime in **c**) as a function of the non-dimensional diameter ratio (D_{stalk}/D_{sphere}). The error bars are based on standard deviation.

causing the vicinity of the initially axisymmetric cusp to buckle into a structure with n-fold symmetry.

Plotting n as a function of D_{stalk}/D_{sphere} for apples (Gala, Honeycrisp and Red Delicious) and for simulations and gels, we find a roughly linear relationship between these parameters for the physical gel swelling experiments, finite element simulations and apples, although apples show a larger slope probably because of the confounding influence of carpel anatomy (Fig. 3e).

To extend this idea to other drupe fruits that also show singular cusps, we plotted the number of cusps in peaches, apricots, cherries and plums as a function of their D_{stalk}/D_{sphere} ratios, and we see that the results are similar to those observed with gels, simulations and single cusps in apples (Supplementary Fig. 5).

All together, our analysis of a biological cusp complements its geometric universality with a morphogenetic perspective on the origin of its shape. We further show how an axisymmetric cusp can become mechanically unstable and form multiple cusps. Our study naturally raises a number of further questions including the nature and dynamics of the molecular signals that trigger the inhibition of growth near the stalk, and the mechanisms linking cell number, cell size and cell shape to tissue morphogenesis, even as the apple within arm's reach continues to beckon.

Online content

Any methods, additional references, Nature Research reporting summaries, source data, extended data, supplementary information, acknowledgements, peer review information; details of author contributions and competing interests; and statements of data and code availability are available at https://doi.org/10.1038/s41567-021-01335-8.

Received: 15 September 2020; Accepted: 20 July 2021;
Published online: 4 October 2021

References

1. Eggers, J. & Fontelos, M. A. *Singularities: Formation, Structure, and Propagation* Vol. 53 (Cambridge Univ. Press, 2015).
2. Thom, R. *Structural Stability and Morphogenesis* (Benjamin, 1975).
3. Arnol'd, V. I. *Catastrophe Theory* (Springer Science & Business Media, 2003).
4. Gilbert, S. F. *Developmental Biology* 10th edn (Sinauer Associates, 2013).
5. Herremans, E. et al. Spatial development of transport structures in apple (*Malus× domestica* Borkh.) fruit. *Front. Plant Sci.* **6**, 679 (2015).

6. Nitsch, J. The physiology of fruit growth. *Annu. Rev. Plant Physiol.* **4**, 199–236 (1953).
7. Bain, J. M. & Robertson, R. The physiology of growth in apple fruits I. Cell size, cell number, and fruit development. *Aust. J. Biol. Sci.* **4**, 75–91 (1951).
8. Janssen, B. J. et al. Global gene expression analysis of apple fruit development from the floral bud to ripe fruit. *BMC Plant Biol.* **8**, 16 (2008).
9. Hugh Smith, W. The histological structure of the flesh of the apple in relation to growth and senescence. *J. Pomol. Hort. Sci.* **18**, 249–260 (1941).
10. Smith, W. H. Cell-multiplication and cell-enlargement in the development of the flesh of the apple fruit. *Ann. Bot.* **14**, 23–38 (1950).
11. Tukey, H. & Young, J. O. Gross morphology and histology of developing fruit of the apple. *Bot. Gaz.* **104**, 3–25 (1942).
12. Reeve, R. Histological investigations of texture in apples. II. Structure and intercellular spaces. *J. Food Sci.* **18**, 604–617 (1953).
13. Jing, S. & Malladi, A. Higher growth of the apple (*Malus*× *domestica* Borkh.) fruit cortex is supported by resource intensive metabolism during early development. *BMC Plant Biol.* **20**, 75 (2020).
14. Karpitschka, S., Eggers, J., Pandey, A. & Snoeijer, J. H. Cusp-shaped elastic creases and furrows. *Phys. Rev. Lett.* **119**, 198001 (2017).
15. Tallinen, T. et al. On the growth and form of cortical convolutions. *Nat. Phys.* **12**, 588–593 (2016).
16. *ABAQUS Analysis User's Manual* (Dassault Systèmes Simulia, 2014).
17. Yao, J.-L. et al. Ectopic expression of the PISTILLATA homologous MdPI inhibits fruit tissue growth and changes fruit shape in apple. *Plant Direct.* **2**, 1–11 (2018).

Publisher's note Springer Nature remains neutral with regard to jurisdictional claims in published maps and institutional affiliations.

© The Author(s), under exclusive licence to Springer Nature Limited 2021

Methods

Experiments with apples and other fruits. To experimentally follow the formation of the apple cusp, we picked apples at various growth stages in the orchard of Peterhouse, University of Cambridge, UK, during June 2018. The profile of the cusp was imaged after longitudinally cutting the apples at the stalk. The profiles of the apple cusps were measured as a function of the pseudo-ontogenetic time (t, where the diameter of the apple served as a proxy to determine its stage of growth[5]), by setting the origin at the stalk, which is shown in Extended Data Fig. 1. To study multi-cusp apples as well as the cusp profiles of other fruits, we purchased them from local grocery stores. The number of cusps were determined by imaging the top view of the fruits (apples, plums, peaches, apricots and cherries), and D_{stalk}/D_{sphere} ratios were obtained from the side views of the fruits obtained by cutting them into halves at the stalk.

Experimental protocol for gel experiments. To ensure that the physical gel models mimic the apple cusp growth, we used two polymers with dissimilar swelling properties when immersed in a solvent (hexane, ≥98.5%; Sigma Aldrich). The bulk of the spherical fruit model was made out of PDMS (SYLGARD 184; Dow Corning); to mimic the stalk region of the fruit, a fluoroelastomer (SIFEL8070A/B, a two-component gel; Shin-Etsu Chemical) was used. PDMS was mixed in a base/cross-linking agent ratio of 40:1, coloured using a red pigment (Silc Pig, Smooth-On) to enhance visibility and degassed to remove all the bubbles generated from mixing. Likewise, SIFEL8070 was mixed in a 1:1 (A:B) ratio and a green pigment (Silc Pig, Smooth-On) was added to it and also degassed. Commercially purchased spherical silicone mould trays with a bottom and lid, both having hemispherical cavities (diameter of each cavity, 12 or 38 mm), were sprayed with a mould release lubricant (Stoner, E218). A fine-pointed needle was used to deposit small volumes (1–10 µl) of SIFEL8070 at the centres of the hemispherical cavities in the bottom tray. Degassed PDMS was then gently poured over the SIFEL8070 drop in the bottom tray, followed by gently covering with the tray top. The lid of the mould tray was pressed to remove excess PDMS and pressed with uniform weights, followed by resting at room temperature for another 30 min to allow the release of bubbles. The mould trays with polymers were then heated in an oven at 75 °C for 2 h followed by curing at 65 °C overnight. The cured PDMS spheres with the stalk region made of SIFEL8070 were gently removed from the mould and swelled in hexane in a transparent rectangular container with time-lapse imaging. Varying the amount of SIFEL8070 gave rise to stalks of different diameters. For the laser sheet imaging experiments, polyethylene fluorescent spheres (0.3 w/w%; diameter, ~35–40 µm; Cospheric UVPMS-BR-0.995) instead of the silicone pigment were mixed with PDMS, degassed and then cured in the oven. The prepared fruit model made of PDMS and its stalk region made with SIFEL8070 were perfectly bonded with each other.

To study the growth-induced cusp formation in the gel models, the cured gel hybrids were immersed in containers filled with hexane. For the smaller spheres (diameter, 12 mm), the swelling occurred over 100 min; for the larger spheres (diameter, 38 mm), the swelling occurred over 20 h. To observe the number of cusps after the desired time for swelling, the samples were taken out of the containers and immediately imaged. For the time-course experiments performed to track the shape of the cusp during the growth (swelling), its cross-section was visualized using a laser sheet (GEM 532). The fluorescent particles embedded in PDMS highlighted the edge of the growing gel model during swelling, which was tracked using ImageJ 1.53c/Fiji software and analysed in MATLAB 2018b.

Numerical simulations. Based on the laser sheet profile of the swelling gel model, we define a smoothly distributed growth rate within the hemispherical model. Here d_{cr} and R_{cr} represent the radius of the stalk zone and non-swelling core zone, respectively. The parameters used in the simulations are $d_a = 1$, $d_b = \sim 3–5$, $k_R = \sim 30–50$, $R_{cr}/R_0 = \sim 0.6–0.9$, $k_d = 50$, $d_{cr} = \sim 0.08–0.60$ and $d_0 = R_0\sqrt{1/d_a^2 + 1/d_b^2}$. For different stalk sizes ($D_{stalk} = 2d_{cr}$), we adjust the corresponding parameters d_b and k_d to ensure the growth rate distribution in accordance with the laser sheet profiles from the experiments. For an axisymmetric hemispherical model, we prescribe a differential growth distribution with a fixed non-swelling zone (Extended Data Fig. 2a). Furthermore, noting that the growth front might move inwards so that the gel sphere swells from the outside to the inside, we separate the growth process into multiple steps—with a different R_{cr} value in each step representing the location of the growth front (Extended Data Fig. 2b) corresponding to an axisymmetric moving zone of material addition except in the neighbourhood of the stalk. For axisymmetric simulations, we used three steps with the growth front moving from $R_{cr}/R_0 = 0.9$ to $R_{cr}/R_0 = 0.7$, as shown in Extended Data Fig. 2a,b. This assumption is to ensure that the outer epidermal layer stops growing after the initial stages of growth. Similar parameters are used in the three-dimensional hemispherical model, where a four-step growth process is assumed (Extended Data Fig. 2c,e).

To verify the scaling law in the theoretical analysis and experiments, we first construct an axisymmetric hemispherical model with 5,400 axisymmetric solid elements (CAX8RH) for both swelling and non-swelling zones. We avoid self-contact near the stalk region $d_{cr} = 0.08$ and 0.10 and introduce numerical damping to relax the integrated energy density towards the minima. In phase I, only the outer epidermal layer is assumed to grow with a strictly fixed axis; in phase II, the outermost layer is assumed to stop growing, while growth is assumed to mainly occur in the intermediate layer as the vertical displacement along the main axis of the hemisphere is relaxed. While our theoretical framework has assumed that the apple tissue is incompressible, assuming a compressible Neo-Hookean material to model the gel and apple flesh[18] with $K = 1.2–2.0\mu$ does not change our qualitative conclusions: we still get the same self-similar profile.

To investigate the formation of multiple cusps in fruits with a large stalk, we construct a three-dimensional hemispherical model with over 70,000 tetrahedron elements (C3D4H). The model is partitioned into swelling and non-swelling zones with a modulus ratio of these zones set as 0.7:1.0 (ref. [19]). The radius of the stalk is $d_{cr} = 0.1$, 0.2, 0.3, 0.4, 0.5 and 0.6. We impose random or sinusoidal initial imperfections with an amplitude of $0.01R_0$ around the stalk region to mimic real defects, as shown in Extended Data Fig. 2c. For each model, the outer surface is carefully partitioned into three parts: a growth-inhibited stalk zone, a slightly disturbed neighbourhood and the rest of the surface, which is in accordance with the prescribed growth profile. Extended Data Fig. 3a depicts the formation of cusps during the growth of an axisymmetric model simulated by the finite element method, with the plan and side views of the hoop (compressive) stress ($\sigma_{\theta\theta}$) profiles shown for the model with eight cusps. These stresses are responsible for the formation of multiple cusps. Additional evidence from the gel swelling experiments corroborate the presence of these stresses, where the swollen gel models cut through the central 'stalk' region leading to the halves folding inwards, as shown by the two examples ($n = 3$ and $n = 8$) in Extended Data Fig. 3b.

Reporting Summary. Further information on research design is available in the Nature Research Reporting Summary linked to this article.

Data availability

Source data are provided with this paper. All other data that support the plots within this paper and other findings of this study are available from the corresponding author upon reasonable request.

Code availability

Source codes to plot the graphs are provided with this paper.

References

18. Grotte, M., Duprat, F., Piétri, E. & Loonis, D. Young's modulus, Poisson's ratio, and Lame's coefficients of golden delicious apple. *Int. J. Food Prop.* **5**, 333–349 (2002).
19. Hu, Y., Chen, X., Whitesides, G. M., Vlassak, J. J. & Suo, Z. Indentation of polydimethylsiloxane submerged in organic solvents. *J. Mater. Res.* **26**, 785–795 (2011).

Acknowledgements

We acknowledge support from the Swiss National Science Foundation (T.C.T.M.); Peterhouse, Cambridge (T.C.T.M.); the China Scholarship Council (file no. 201906210341); NSF DMR-2011754 (L.M.); NSF DMR-1922321 (L.M.); NSF DMS 1764269 (L.M.); and the Henri Seydoux Fund (L.M.).

Author contributions

L.M. conceived of the problem and designed the study and approaches. A.C. developed and performed the swelling experiments of the physical gel models. T.C.T.M. and L.M. developed the theoretical models. T.C.T.M. performed the apple cross-section measurements. S.Y. performed the finite element simulations of growth. E.S. numerically solved the eikonal equation. A.C., T.C.T.M. and L.M. wrote the paper. L.M. supervised the study.

Competing interests

The authors declare no competing interests.

Additional information

Extended data is available for this paper at https://doi.org/10.1038/s41567-021-01335-8.

Supplementary information The online version contains supplementary material available at https://doi.org/10.1038/s41567-021-01335-8.

Correspondence and requests for materials should be addressed to L. Mahadevan.

Peer review information *Nature Physics* thanks the anonymous reviewers for their contribution to the peer review of this work.

Reprints and permissions information is available at www.nature.com/reprints.

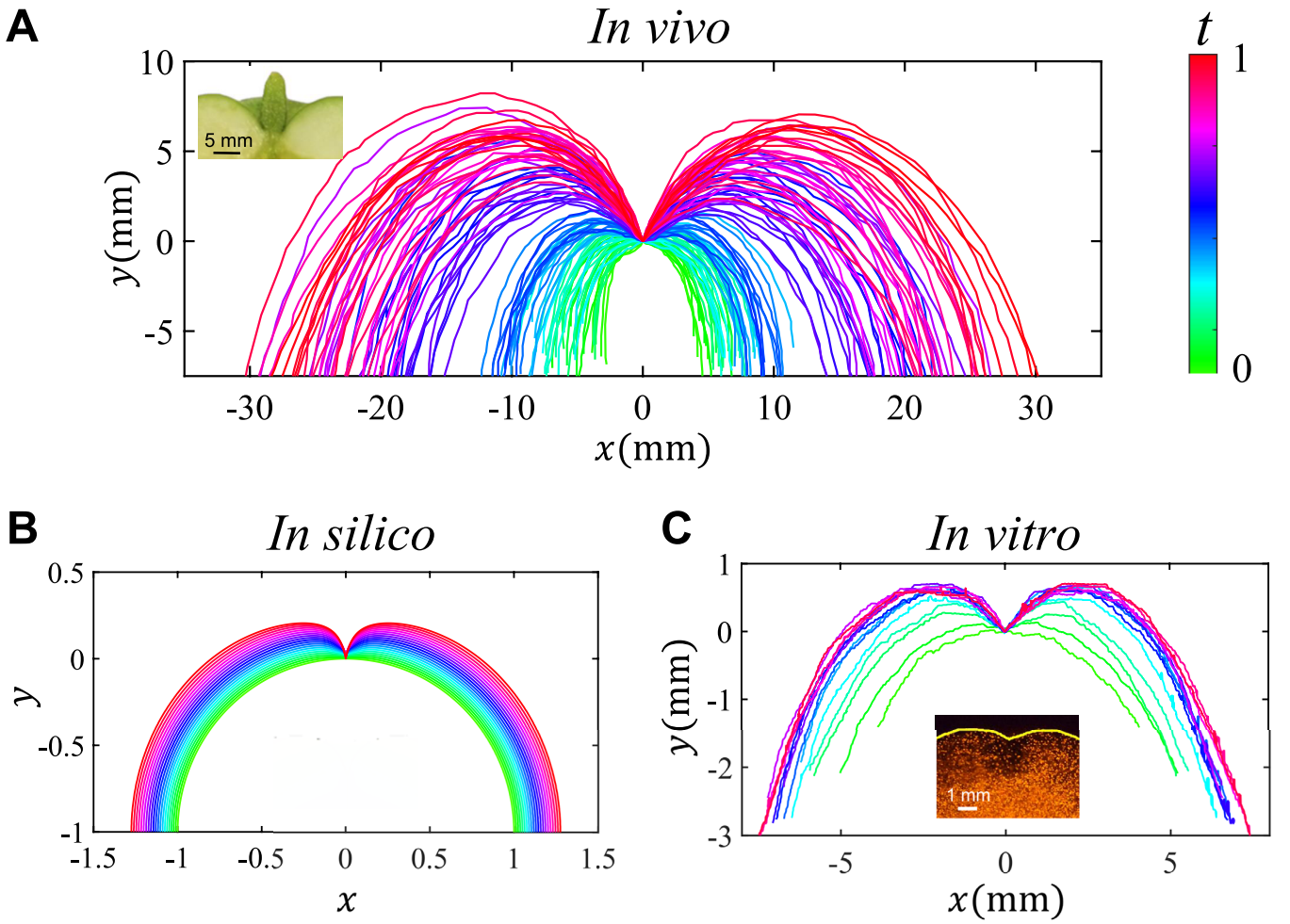

Extended Data Fig. 1 | Raw and collapsed cusp profiles for apples, simulations and physical gel models. (A) *In vivo*: Experimental measurements of profiles near the cusp of apple cross-sections at different stages of growth. 2 pickings of the apples were made in June 2018. At the time of picking, the fruits were cut through the middle at the stalk, (0,0), and images of the cross section were taken. The apple profile was traced from the images of 100 apples at different stages of growth. The colors indicate time point (t) during growth, where t represents the normalized time scale for cusp growth in apples. The inset shows an apple cusp at $t=1$. (B) *In silico*: Simulation profiles as a function of time. The inset shows a cusp at $t=0.5$. (C) *In vitro*: Gel profiles of the cusp obtained from laser sheet experiments as a function of time, going from 0 min to 130 min, where t represents the normalized time with respect to the total time of the experiment, that is 130 min. The inset shows a cusp at $t=0.8$.

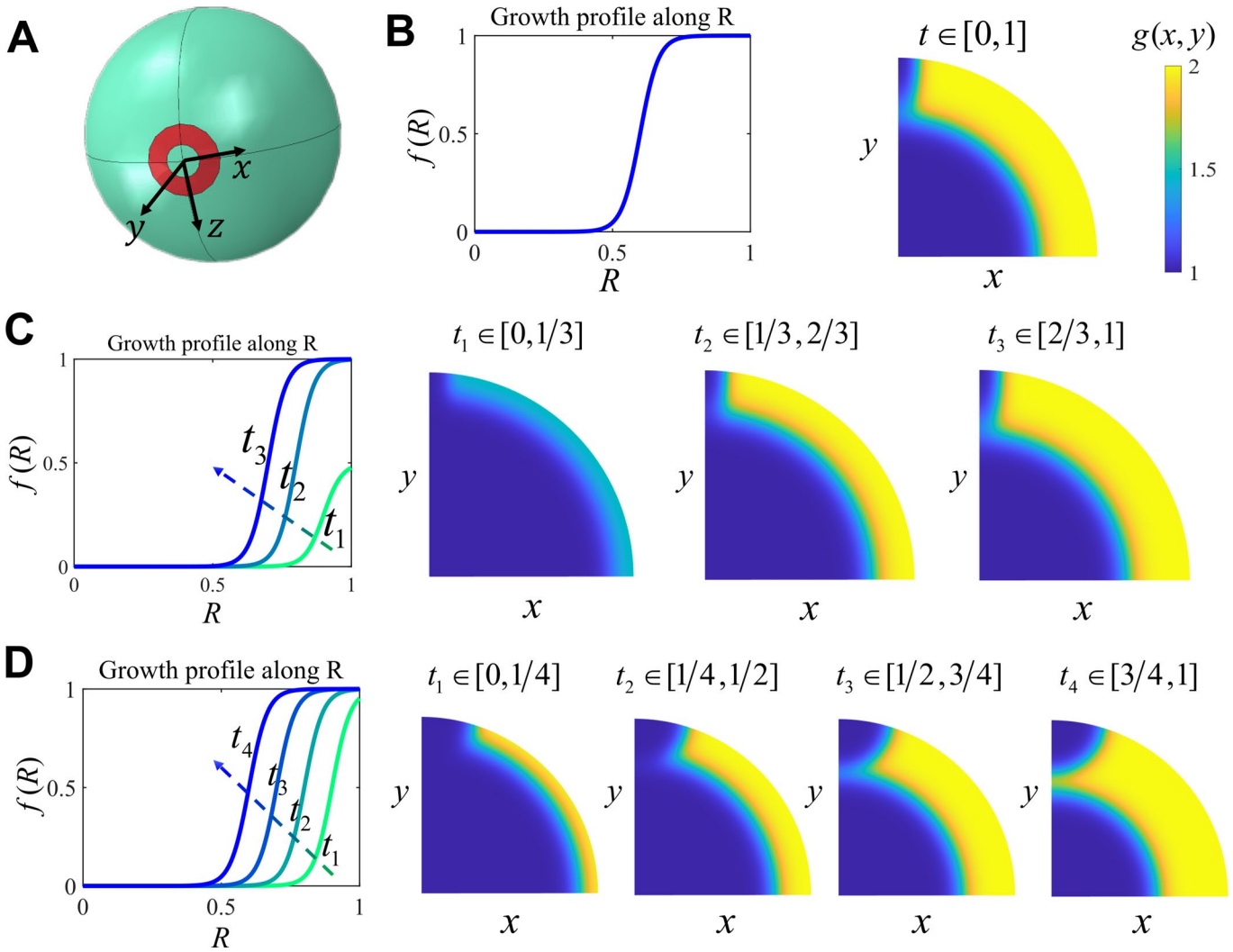

Extended Data Fig. 2 | Description of FEM model and growth profiles. (A) Three dimensional model illustration for the FEM simulations. (B) For the cusp formation in 2D FEM simulations, the growth profile along radius, $f(R)$, is assumed in the form of a sigmoid function. (Right): Growth distribution for single cusp formation in asymmetric geometry for FEM simulations. The swelling and non-swelling zone are fixed throughout the process. To model the isotropic inhomogeneous growth we use the following profile: $\mathbf{G} = g(x,y,t)\mathbf{I}$, where the growth rate is given by $g(x,y,t) = 1 + f(R)h(d)t$, with $f(R) = \{1 + \exp[-k_R(R - R_{cr})/R_0]\}^{-1}$, and $h(d) = \{1 + \exp[-k_d(d - d_{cr})/d_0]\}^{-1}$. Here $R = \sqrt{x^2 + (R_0 + y)^2}$ and $d = \sqrt{x^2/d_a^2 + y^2/d_b^2}$. This growth profile allows g to vary smoothly from $g = 1$ in the core and the neighborhood of the stalk to $g > 1$ in the growing cortex. (C) The growth profile, $f(R)$, moves inwards as a function of time in 2D simulations for the formation of a single cusp at times $t_1 - t_3$. (Right): Growth profile for single cusp formation with a moving swelling zone for each time interval $t_1 - t_3$. (D) For the cusp formation in 3D FEM simulations, the growth profile, $f(R)$, moves inwards as a function of time at time points $t_1 - t_4$. (Right): Growth profile used in 3D FEM simulations ($D_{stalk}/D_{sphere} = 0.3$) for each corresponding time intervals.

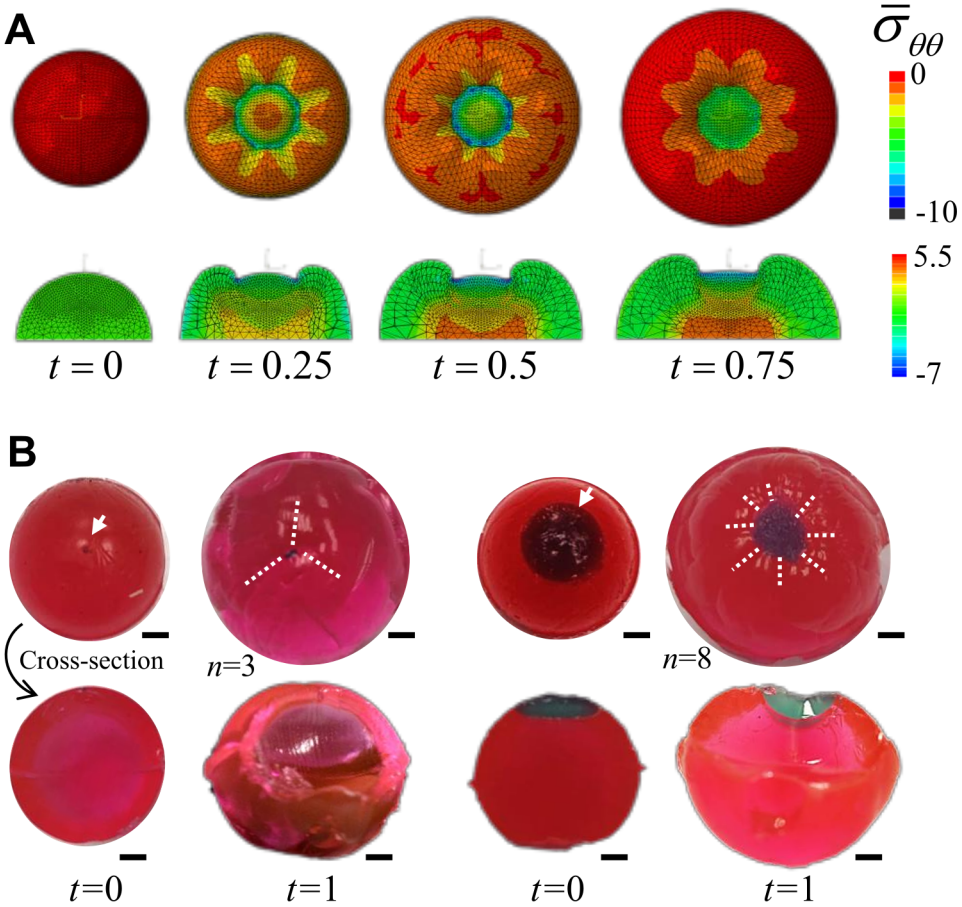

Extended Data Fig. 3 | Stress distribution in FEM simulations and gel models for multicusp formation. (A) Plan view and cross-section from FEM simulations with $n=8$ cusps showing temporal evolution of the compressive stresses around the central stalk region, which are responsible for the formation of the multiple cusps. Respective color legends shows the magnitude and sign of the Hoop stress. (B) Two examples of gel models, one with a small non-swelling stalk (left, $D_{stalk}/D_{sphere} = 0.05$) and a large stalk (right, $D_{stalk}/D_{sphere} = 0.5$) denoted by arrows. At $t=0$, both these gel models were cut through their mid-plane to show their cross-section before swelling. Both the halves remain flat after cutting showing no pre-stresses in the samples. A replicate of the model for each case is swelled in hexane until it develops the cusp. At $t=1$ (75 min of swelling reaching the final cusped state), when the swollen gel spheres are cut into halves, each of these fold inwards demonstrating the presence of compressive hoop stresses in the outer region. These hoop stresses are responsible for formation of multiple cusps when D_{stalk}/D_{sphere} is large. All scale bars denote 2 mm. The white dashed lines are guide to the eyes at locations where the cusps are observed before longitudinally slicing them.

nature portfolio

Corresponding author(s): L. Mahadevan

Last updated by author(s): Jul 4, 2021

Reporting Summary

Nature Portfolio wishes to improve the reproducibility of the work that we publish. This form provides structure for consistency and transparency in reporting. For further information on Nature Portfolio policies, see our Editorial Policies and the Editorial Policy Checklist.

Statistics

For all statistical analyses, confirm that the following items are present in the figure legend, table legend, main text, or Methods section.

n/a	Confirmed
☐	☒ The exact sample size (*n*) for each experimental group/condition, given as a discrete number and unit of measurement
☒	☐ A statement on whether measurements were taken from distinct samples or whether the same sample was measured repeatedly
☒	☐ The statistical test(s) used AND whether they are one- or two-sided *Only common tests should be described solely by name; describe more complex techniques in the Methods section.*
☒	☐ A description of all covariates tested
☒	☐ A description of any assumptions or corrections, such as tests of normality and adjustment for multiple comparisons
☒	☐ A full description of the statistical parameters including central tendency (e.g. means) or other basic estimates (e.g. regression coefficient) AND variation (e.g. standard deviation) or associated estimates of uncertainty (e.g. confidence intervals)
☒	☐ For null hypothesis testing, the test statistic (e.g. *F*, *t*, *r*) with confidence intervals, effect sizes, degrees of freedom and *P* value noted *Give P values as exact values whenever suitable.*
☒	☐ For Bayesian analysis, information on the choice of priors and Markov chain Monte Carlo settings
☒	☐ For hierarchical and complex designs, identification of the appropriate level for tests and full reporting of outcomes
☒	☐ Estimates of effect sizes (e.g. Cohen's *d*, Pearson's *r*), indicating how they were calculated

Our web collection on statistics for biologists contains articles on many of the points above.

Software and code

Policy information about availability of computer code

Data collection	This information is already provided in the text and SI.
Data analysis	This is already provided in the text and SI. We used ABAQUS, a commercial FEM package, and MATLAB, a commercial data analysis toolbox.

For manuscripts utilizing custom algorithms or software that are central to the research but not yet described in published literature, software must be made available to editors and reviewers. We strongly encourage code deposition in a community repository (e.g. GitHub). See the Nature Portfolio guidelines for submitting code & software for further information.

Data

Policy information about availability of data

All manuscripts must include a data availability statement. This statement should provide the following information, where applicable:

- Accession codes, unique identifiers, or web links for publicly available datasets
- A description of any restrictions on data availability
- For clinical datasets or third party data, please ensure that the statement adheres to our policy

All data are available upon request from the corresponding author.

Field-specific reporting

Please select the one below that is the best fit for your research. If you are not sure, read the appropriate sections before making your selection.

☒ Life sciences ☐ Behavioural & social sciences ☐ Ecological, evolutionary & environmental sciences

For a reference copy of the document with all sections, see nature.com/documents/nr-reporting-summary-flat.pdf

Life sciences study design

All studies must disclose on these points even when the disclosure is negative.

Sample size	Described in the text already.
Data exclusions	No data were excluded.
Replication	N/A
Randomization	N/A
Blinding	N/A

Reporting for specific materials, systems and methods

We require information from authors about some types of materials, experimental systems and methods used in many studies. Here, indicate whether each material, system or method listed is relevant to your study. If you are not sure if a list item applies to your research, read the appropriate section before selecting a response.

Materials & experimental systems

n/a	Involved in the study
☒	☐ Antibodies
☒	☐ Eukaryotic cell lines
☒	☐ Palaeontology and archaeology
☒	☐ Animals and other organisms
☒	☐ Human research participants
☒	☐ Clinical data
☒	☐ Dual use research of concern

Methods

n/a	Involved in the study
☒	☐ ChIP-seq
☒	☐ Flow cytometry
☒	☐ MRI-based neuroimaging